ISSN 0021-3640, JETP Letters, 2023, Vol. 117, No. 7, pp. 498–503. © The Author(s), 2023. This article is an open access publication.
Russian Text © The Author(s), 2023, published in Pis'ma v Zhurnal Eksperimental'noi i Teoreticheskoi Fiziki, 2023, Vol. 117, No. 7, pp. 498–503.

OPTICS
AND LASER PHYSICS

High-Quality Infrared Metalenses Based on Germanium Dimers

V. M. Pustynnikova[a], A. I. Musorin[a], and A. A. Fedyanin[a,*]

[a] *Faculty of Physics, Moscow State University, Moscow, 119991 Russia*

**e-mail: fedyanin@nanolab.phys.msu.ru*

Received February 22, 2023; revised February 23, 2023; accepted March 2, 2023

Modern methods of nanophotonics allow creating miniature devices that change the direction of light propagation, modulate the phase front, and control the outcoming state of the polarization. One of the promising areas of research is the development of flat optics elements based on planar analogues of metamaterials—dielectric metasurfaces, which are two-dimensional arrays of subwavelength nanoparticles with a high refractive index and low absorption coefficient. However, the resonances of such nanoscatterers have usually a low quality factor. Symmetry breaking of particle can lead to the excitation of a high-Q quasi-bound states in the continuum. In this work, we numerically study infrared metasurfaces that support such resonances and are formed by dimers of germanium nanocuboids. The possibility of focusing radiation to a point and line by 300-nm-thick spherical and cylindrical metalenses is shown.

DOI: 10.1134/S0021364023600556

The approach of planar optics compatible with microelectronic circuit technologies and integrated optoelectronic components makes the idea of a photonic lab on a chip more realistic. Ultra-thin analogues of optical components, called metasurfaces [1], are the basis of planar optics (Fig. 1). A metasurface is a two-dimensional ordered array of subwavelength nanoscatterers, called meta-atoms. They can be considered as a source of secondary waves. According to the Huygens–Fresnel principle, the resulting response of the whole structure is interference of these waves. Metasurfaces allow to control the polarization [2], amplitude [3], phase of the transmitted/reflected light [4] as well as its direction of propagation [5, 6] due to the resonant localization of light energy in the volume of nanoparticles or at their edges [7]. Metasurfaces are capable of forming complex wave fronts. This fact is the basis for planar optics elements: wave plates [8], spectral filters [9], polarizers [10], lenses [11]. Recent developments in planar lenses show that spatially ordered resonant scatterers with the desired light phase delay can compensate for chromatic [12] (in three-layer plasmonic disk metasurfaces) and spherical [13] (silicon nano-posts metalens) aberrations, achieve high numerical aperture [14] (silicon cylinder dimers) and make such devices multifunctional [15] (cuboids made of phase-change material). The proper arrangement of the meta-atoms allows the creation of an ultrathin axicon that generates non-diffracting Bessel beams by a metalens formed by gold V-shaped antennas [16]. Further improvements of metasurfaces in general, and metalenses in particular, are realized by the use of materials whose properties are sensitive to external influences: liquid crystals [17–19], magnetics [20, 21], semiconductors [22–24]. Active devices that modulate incident radiation can be created in this way.

One of the disadvantages of meta-devices is the low quality factor of the meta-atoms resonances ($Q \sim 10$). To increase the efficiency of new nanophotonics devices it has been proposed to form a metasurface of nanoparticles supporting bound states in the continuum resonances [25]. Such modes are formed by spectral overlap of two resonances, usually "dark" and "bright." This allows one to control the amount of radiative losses leading to narrowing the resonance features and increasing the quality factor to values of $Q \sim 10^2$–10^3. Dark resonances mean that they cannot be excited or detected in the far diffraction zone, i.e., that they have no radiative losses. Bound states in the continuum are configurations of electromagnetic fields that exist in a continuous spectrum but remain localized spatially. Such examples have been studied in a wide range of material systems: in piezoelectric materials, dielectric photonic crystals, optical waveguides and fibers, quantum dots, graphene, and topological insulators [26]. Bound states in the continuum

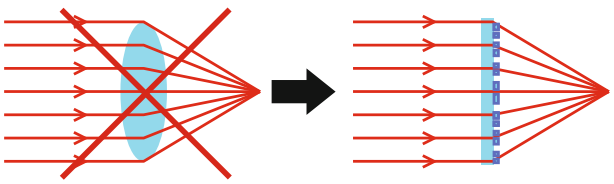

Fig. 1. (Color online) Schematic representation of a miniature planar lens based on a metasurface.

Table 1. Number of periods forming a given phase zone of a planar metalens

Phases	0	$-\frac{\pi}{4}$	$-\frac{2\pi}{4}$	$-\frac{3\pi}{4}$	$-\pi$	$-\frac{5\pi}{4}$	$-\frac{6\pi}{4}$	$-\frac{7\pi}{4}$	-2π	$-\frac{9\pi}{4}$	$-\frac{10\pi}{4}$	$-\frac{11\pi}{4}$
Number	12	9	6	5	4	4	3	3	3	3	3	3
Phases	-3π	$-\frac{13\pi}{4}$	$-\frac{14\pi}{4}$	$-\frac{15\pi}{4}$	-4π	$-\frac{17\pi}{4}$	$-\frac{18\pi}{4}$	$-\frac{19\pi}{4}$	-5π	$-\frac{21\pi}{4}$	$-\frac{22\pi}{4}$	$-\frac{23\pi}{4}$
Number	2	2	2	2	2	2	2	2	2	2	2	2

resonances manifest themselves in the response of single particles [27] and metasurfaces [28, 29]. The presence of asymmetry plays an essential role for the realization of high-quality resonances in arrays of particle, because it allows making resonances of dark modes bright [30]. Examples of asymmetry include missing part of a cuboid [31], and shift of a hole from the center in a magnetic dielectric nanodisk to enhance magneto-optical effects [32]. The meta-atom may be a pair of ellipsoids tilted relative to each other vertically to enhance non-linear optical effects [33] or two cuboids [34, 35]. Although nanocubes cannot be made with sharp edges during fabrication, their advantage is the greater number of independent parameters controlling the optical response and extending the ability to tune the resonant scattering and the directional pattern through variation of the amplitude and the phase of the incident waves.

In the present work, it is proposed to use high-quality metasurfaces for realization of ultra-thin elements of infrared planar optics—cylindrical and spherical metalenses. Metasurfaces with bound state in the continuum resonances for radiation focusing have been examined slightly [35, 36]. Therefore, in this paper an asymmetric dimer of cuboids is considered as a meta-atom. The majority of studies on planar optics consider devices and materials for the visible range (silicon, titanium dioxide, etc.). In this work, the metasurface is simulated for the infrared range with the working wavelength of $\lambda = 1.8$ μm, and germanium is taken as a material with a large refractive index and low absorption coefficient at this spectral region.

The focusing properties of the metasurface are determined by the spatial profile of the transmitted wave phase, which depends on the focal distance f and the wavelength of light λ. For radiation propagating along the Z axis, the value of a phase delay φ depends on the position of the meta-atom (x, y):

$$\varphi(x, y) = \frac{2\pi}{\lambda}\left(\sqrt{f^2 + x^2 + y^2} - f\right). \quad (1)$$

This continuous function is shown by the black line in Fig. 2a at $y = 0$ and the cyan surface in Fig. 2b. The phase difference between the center and edges of the metalens must be $2\pi m$, $m = 1,2,...$ in order to amplify waves at the focal plane. The greater the order of m, the more effective the focusing is. To realize the phase profile (1) in practice, one needs to discretize the function $\varphi(x, y)$. The interval $0...2\pi$ is divided evenly with a step of $\pi/4$, and eight configurations of meta-atoms that realize the desired phase delays should be found. For the values $\varphi_1 = (0 \pm \pi/8)$ the phase is assumed to be zero, the region $\varphi_2 = (\pi/4 \pm \pi/8)$ corresponds to $\pi/4$ delay, etc. Values greater than 2π are reduced to the $0...2\pi$ interval by subtracting $2\pi m$. By substituting the values of the angle φ_k into the expression (1), one can find the coordinates of the boundaries and the width of the phase zone formed by the meta-atoms of the same configuration. Then one can calculate the number of cells that form this region, depending on the period of the metalens array. This is the way for the phase discretization procedure. An example of the discretization is shown in Figs. 2a, 2b for the wavelength of $\lambda = 1.8$ μm, focal length of $f = 500$ μm, period of $P = 0.88$ μm and $m = 3$. Table 1 shows the number of cells forming a zone with a certain phase.

Numerical simulation is performed by the finite-difference time-domain method. The light is incident along the Z axis, polarization is along the Y axis (see Fig. 2c). A substrate is a dielectric with the refractive index of $n = 1.4$. The calculation is performed in several steps. The first one is the selection of meta-atom configurations that gives the desired phase delay and has as large transmittance as possible, ideally—unity. The three-dimensional computational domain is bounded by perfectly matched layers (PML) along the Z axis, and periodic conditions along the X and Y axes. The parameters of the studying problem are two widths and two lengths of couple cuboids forming the asymmetric meta-atom dimer, period and height. Taking into account typical fabrication process of semiconductor nanoparticles, it is reasonable to keep the height of the whole metalens uniform. The situation that some particles are higher than others is not considered. The particle height h is 300 nm, and the optimal square lattice period is $P_x = P_y = 880$ nm. Figure 3 shows an example of meta-atom with parameters (x_l, y_l); $(x_r, y_r) = (450, 445)$ nm; (200, 700) nm: (a) transmittance spectrum, (b) spectrum of the phase of the transmitted wave; (c) distribution of the absolute value of the local electric field plotted in the XY plane at the half height of the nanoparticle. The phase in the text refers to the phase difference between the transmitted the metasurface wave and incident

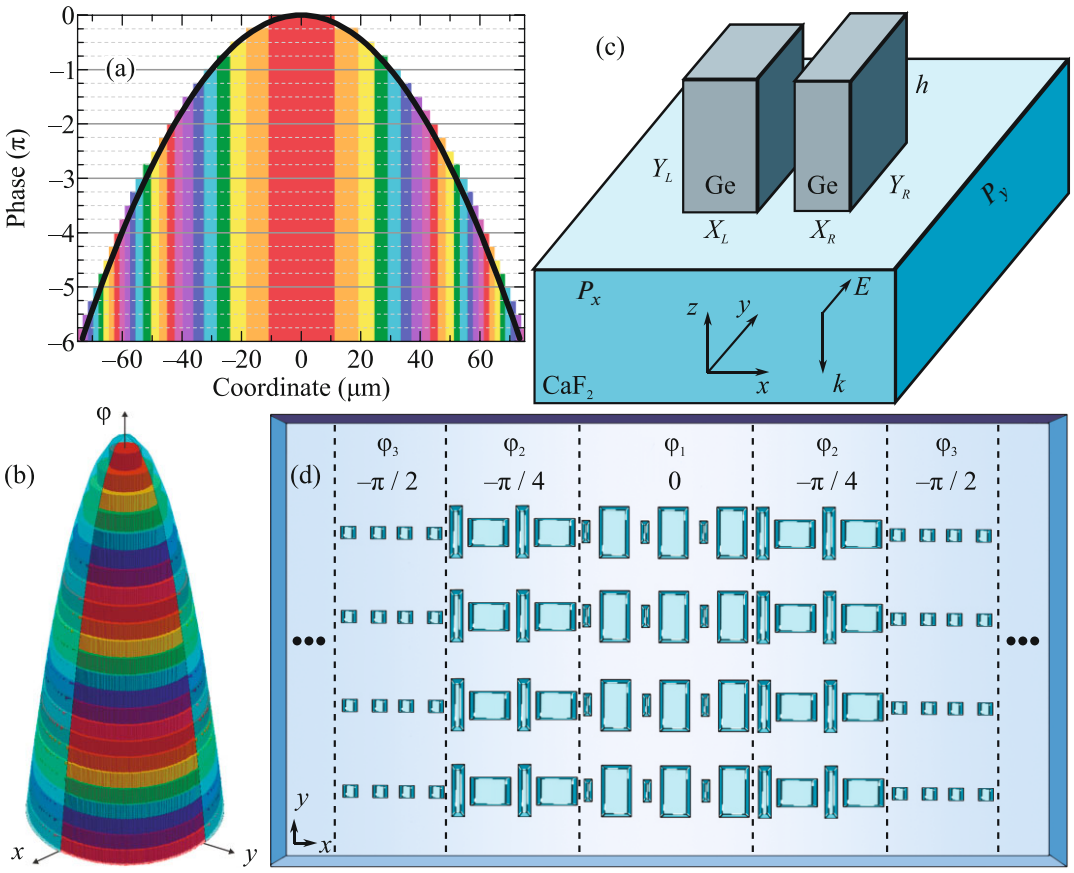

Fig. 2. (Color online) (a, b) Dependence of the phase delay of the light wave passed the metalens on the position of the meta-atom. The black line in (a) and the cyan paraboloid in (b) are obtained from the expression (1); the colored columns—phase values with π/4 step. (c) Studying geometry of the meta-atom—the unit cell of the metalens. (d) Schematic representation of a cylindrical metalens.

one. There is a mode at the wavelength of 1.8 μm within a wide dip in the transmittance spectrum (Fig. 3a) whose quality factor is equal to 100 and value of transmittance reaches of 0.7. The field distribution (Fig. 3c) for this spectral position shows that the maximum energy concentrates outside the dimer particles, which explains a relatively high transmittance and a field enhancement of up to 20 times. The phase value equals to π (Fig. 3b). There is another resonance near the wavelength of 1.65 μm with near unity transmission and a phase value of π/2.

Variation of the widths and lengths of the cuboids allows to specify eight configurations of the meta-atoms with the demanded phase delays. The cuboids sizes and corresponding phases are shown in Fig. 4. The center of each cuboid is placed in the middle of the meta-atom along the *Y*-axis (440 nm), while along the *X*-axis in a quarter (220 nm) and three quarters (660 nm) of the period. The distance between the centers of the cuboids is fixed and equals to half of the period, while the gap between the particles is determined by the widths of the particles.

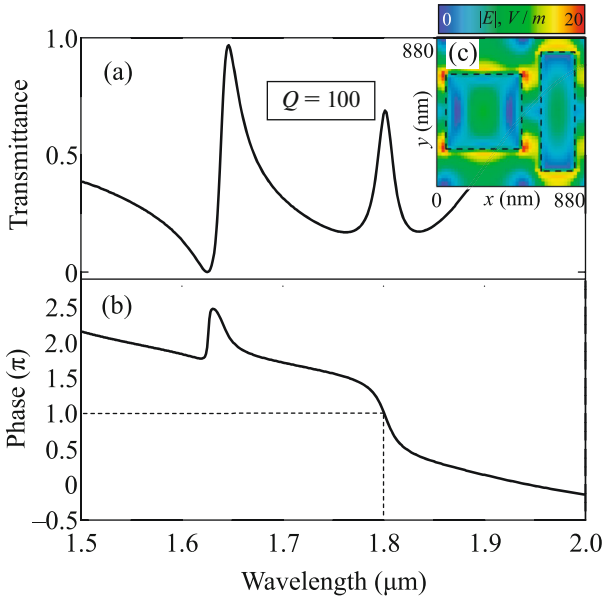

Fig. 3. (Color online) (a) Transmittance spectrum of the meta-atom (x_l, y_l); (x_r, y_r) = (450, 445); (200, 700) nm: T (1.8 μm) = 0.7; (b) spectrum of the phase of the transmitted wave, φ (1.8 μm) = π; (c) distribution of the absolute value of local electric field for the wavelength of λ = 1.8 μm.

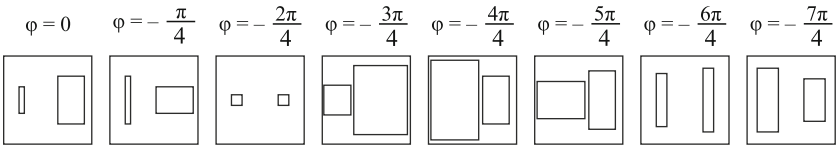

X_L (nm)	100	100	100	225	450	450	100	200
Y_L (nm)	300	500	100	280	750	350	500	600
X_R (nm)	300	400	100	505	250	250	100	200
Y_R (nm)	500	300	100	650	450	550	600	400

Fig. 4. Phase delays and corresponding schemes of meta-atoms. Sizes of cuboids forming meta-atoms.

Phase zones of the cylindrical metalens are formed by spatially placing the correct number of meta-atoms with an appropriate phase value. Figure 5 shows the final phase dependence on the coordinate along the metalens (black dots). It shows also the theoretical dependence (red line) calculated according to Eq. (1). The results are in good agreement, and the phase discretization is performed correctly.

The second step is calculation of the focusing properties of the metalens. The three-dimensional computational region is bounded by the PML at all axes. The distance between the edges of studying system and boundaries is set to three wavelengths to avoid the influence of back reflections on the optical response of the model. Figure 6 shows the results of calculation in the far diffraction zone. Figures 6a, 6c shows the distribution of the electric field intensity along the propagation path. There is a bright spot near the focal plane ($f = 500$ μm) caused by the constructive interference of waves from phase zones, i.e., focusing. The right panels of Fig. 6 show the electric field intensity distribution in the focal plane if the phase zones are arranged as circles to form a spherical lens that collects light to the point (Fig. 6b), and as rectangles to form a cylindrical lens that concentrates radiation to the line (Fig. 6d). The full width at half maximum of the intensity for both lenses is equal to 9 μm. The size of the lenses is 147.84 μm, and it corresponds to the phase delays of 6π.

To conclude, the elements of planar infrared optics that focus radiation in a point and line—spherical and cylindrical metalenses—have been designed. The metalenses are two-dimensional arrays of asymmetric dimers of germanium nanoparticles. The parameters of eight high-quality meta-atoms are tuned up to match phase delays from 0 to 2π with π/4 step by the finite-difference time-domain method for a wavelength of 1.8 μm. For a focal length of 500 μm, the spot size is 9 μm for both lenses. Focusing exists only for

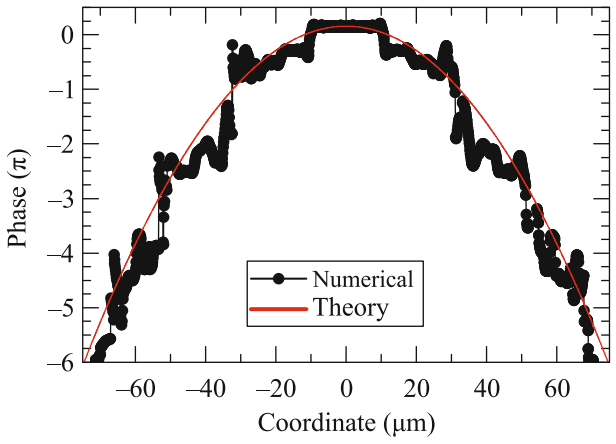

Fig. 5. (Color online) Dependence of the phase of the light wave transmitted the metalens on the position of the meta-atom according to Eq. (1) (red line) and the result of numerical calculation (black dots).

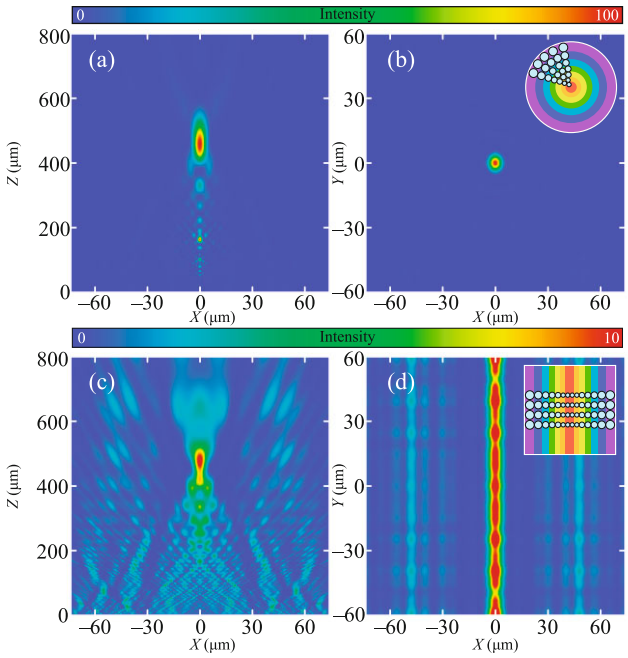

Fig. 6. (Color online) Distribution of the electric field intensity in the following planes: (a, c) XZ plane for $y = 0$; (b, d) XY plane for the focal position of $z = f = 500$ μm. The distributions are obtained for (a, b) spherical and (c, d) cylindrical lenses. The insets of panels (b, d) schematically show the layout of phase zones formed by meta-atoms.

linear polarization of light parallel to the long side of the cuboid, while the other one changes the spectral mode composition of the system, shifts the resonances, and alter phase delays leading to absence of the focusing effect. The obtained results can be used for compact optical devices development of the infrared range, such as scanners, QR-code or bar code readers. They could be interesting for the development of miniaturized fingerprint-based personal identification systems [37].

ACKNOWLEDGMENTS

We are grateful to B.S. Luk'yanchuk for the fruitful discussions.

FUNDING

This work was carried out within the framework of the Development Program of the Moscow State University (interdisciplinary scientific and educational school "Photonic and Quantum Technologies. Digital Medicine") and was supported by the Russian Foundation for Basic Research (project no. 21-52-12036, numerical calculation of focusing) and by the Foundation for the Advancement of Theoretical Physics and Mathematics BASIS (project no. 22-1-3-5-1, calculation of the amplitude-frequency and phase-frequency characteristics of meta-atoms).

CONFLICT OF INTEREST

The authors declare that they have no conflicts of interest.

OPEN ACCESS

REFERENCES

1. N. Yu and F. Capasso, Nat. Mater. **13**, 139 (2014).
2. N. Yu, F. Aieta, P. Genevet, M. A. Kats, Z. Gaburro, and F. Capasso, Nano Lett. **12**, 6328 (2012).
3. T. Ellenbogen, K. Seo, and K. B. Crozier, Nano Lett. **12**, 1026 (2012).
4. A. Arbabi, Y. Horie, M. Bagheri, and A. Faraon, Nat. Nanotechnol. **10**, 937 (2015).
5. M. I. Shalaev, J. Sun, A. Tsukernik, A. Pandey, K. Nikolskiy, and N. M. Litchinitser, Nano Lett. **15**, 6261 (2015).
6. A. D. Gartman, A. S. Ustinov, A. S. Shorokhov, and A. A. Fedyanin, JETP Lett. **114**, 441 (2021).
7. A. I. Kuznetsov, A. E. Miroshnichenko, M. L. Brongersma, Y. S. Kivshar, and B. Luk'yanchuk, Science (Washington, DC, U. S.) **354**, aag2472 (2016).
8. Y. Yang, W. Wang, P. Moitra, I. Kravchenko, D. Briggs, and J. Valentine, Nano Lett. **14**, 1394 (2014).
9. Z. Zheng, A. Komar, K. Z. Kamali, J. Noble, L. Whichello, A. E. Miroshnichenko, M. Rahmani, D. N. Neshev, and L. Xu, J. Appl. Phys. **130**, 053105 (2021).
10. Y. Intaravanne and X. Chen, Nanophotonics **9**, 1003 (2020).
11. M. Khorasaninejad and F. Capasso, Science (Washington, DC, U. S.) **358**, eaam8100 (2017).
12. O. Avayu, E. Almeida, Y. Prior, and T. Ellenbogen, Nat. Commun. **8**, 14992 (2017).
13. A. Arbabi, E. Arbabi, S. M. Kamali, Y. Horie, S. Han, and A. Faraon, Nat. Commun. **7**, 13682 (2016).
14. R. Paniagua-Dominguez, Y. F. Yu, E. Khaidarov, S. Choi, V. Leong, R. M. Bakker, X. Liang, Y. H. Fu, V. Valuckas, L. A. Krivitsky, and A. I. Kuznetsov, Nano Lett. **18**, 2124 (2018).
15. L. Chen, Y. Hao, L. Zhao, R. Wu, Y. Liu, Z. Wei, N. Xu, Z. Li, and H. Liu, Opt. Express **29**, 9332 (2021).
16. F. Aieta, P. Genevet, M. A. Kats, N. Yu, R. Blanchard, Z. Gaburro, and F. Capasso, Nano Lett. **12**, 4932 (2012).
17. A. Komar, R. Paniagua-Dominguez, A. Miroshnichenko, Y. F. Yu, Y. S. Kivshar, A. I. Kuznetsov, and D. Neshev, ACS Photon. **5**, 1742 (2018).
18. M. Bosch, M. R. Shcherbakov, K. Won, H. Lee, Y. Kim, and G. Shvets, Nano Lett. **21**, 3849 (2021).
19. J. Wang, K. Li, H. He, W. Cai, J. Liu, Z. Yin, Q. Mu, V. K. S. Hisao, D. Gérard, D. Luo, G. Li, and Y. J. Liu, Laser Photon. Rev. **16**, 2100396 (2022).
20. A. I. Musorin, M. G. Barsukova, A. S. Shorokhov, B. S. Luk'yanchuk, and A. A. Fedyanin, J. Magn. Magn. Mater. **459**, 165 (2018).
21. A. I. Musorin, A. V. Chetvertukhin, T. V. Dolgova, H. Uchida, M. Inoue, B. S. Luk'yanchuk, and A. A. Fedyanin, Appl. Phys. Lett. **115**, 151102 (2019).
22. P. P. Iyer, M. Pendharkar, and J. A. Schuller, Adv. Opt. Mater. **4**, 1582 (2016).
23. G. K. Shirmanesh, R. Sokhoyan, P. C. Wu, and H. A. Atwater, ACS Nano **14**, 6912 (2020).
24. V. V. Zubyuk, P. P. Vabishchevich, M. R. Shcherbakov, A. S. Shorokhov, A. N. Fedotova, S. Liu, G. Keeler, T. V. Dolgova, I. Staude, I. Brener, and A. A. Fedyanin, ACS Photon. **6**, 2797 (2019).
25. K. Koshelev, A. Bogdanov, and Y. Kivshar, Sci. Bull. **64**, 836 (2019).
26. H. Qin, W. Redjem, and B. Kante, Opt. Lett. **47**, 1774 (2022).
27. E. V. Melik-Gaykazyan, K. L. Koshelev, J. Choi, S. S. Kruk, H. Park, A. A. Fedyanin, and Y. S. Kivshar, JETP Lett. **109**, 131 (2019).

28. V. V. Zubyuk, P. A. Shafirin, M. R. Shcherbakov, G. Shvets, and A. A. Fedyanin, ACS Photon. **9**, 493 (2022).
29. K. I. Okhlopkov, A. Zilli, A. Tognazzi, D. Rocco, L. Fagiani, E. Mafakheri, M. Bollani, M. Finazzi, M. Celebrano, M. R. Shcherbakov, C. Angelis, and A. A. Fedyanin, Nano Lett. **21**, 10438 (2021).
30. K. Koshelev, S. Lepeshov, M. Liu, A. Bogdanov, and Y. Kivshar, Phys. Rev. Lett. **121**, 193903 (2018).
31. S. Campione, S. Liu, L. I. Basilio, L. K. Warne, W. L. Langston, T. S. Luk, J. R. Wendt, J. L. Reno, G. A. Keeler, I. Brener, and M. B. Sinclair, ACS Photon. **3**, 2362 (2016).
32. A. M. Chernyak, M. G. Barsukova, A. S. Shorokhov, A. I. Musorin, and A. A. Fedyanin, JETP Lett. **111**, 46 (2020).
33. A. P. Anthur, H. Zhang, R. Paniagua-Dominguez, D. A. Kalashnikov, S. T. Ha, T. W. Maß, A. I. Kuznetsov, and L. Krivitsky, Nano Lett. **20**, 8745 (2020).
34. K. Koshelev, Y. Tang, K. Li, D. Choi, G. Li, and Y. Kivshar, ACS Photon. **6**, 1639 (2019).
35. A. Archetti, R. Lin, N. Restori, F. Kiani, T. V. Tsoulos, and G. Tagliabue, Nanophotonics **11**, 3969 (2022).
36. E. Klopfer, M. Lawrence, D. Barton III, J. Dixon, and J. A. Dionne, Nano Lett. **20**, 5127 (2020).
37. E. Lassalle, T. W. Mass, D. Eschimese, A. V. Baranikov, E. Khaidarov, S. Li, R. Paniagua-Dominguez, and A. I. Kuznetsov, ACS Photon. **8**, 1457 (2021).

Translated by the authors